Planetary and Space Science 102 (2014) 152–163

Contents lists available at ScienceDirect

Planetary and Space Science

journal homepage: www.elsevier.com/locate/pss

The age of Phobos and its largest crater, Stickney

N. Schmedemann [a,*], G.G. Michael [a], B.A. Ivanov [b], J.B. Murray [c], G. Neukum [a]

[a] Institute of Geological Sciences, Freie Universität Berlin, Berlin, Germany
[b] Institute of Dynamics of Geospheres, Moscow, Russia
[c] Department of Earth Sciences, Open University, Milton Keynes, UK

ARTICLE INFO

Article history:
Received 15 December 2012
Received in revised form
25 February 2014
Accepted 16 April 2014
Available online 26 April 2014

Keywords:
Phobos
Stickney
Crater retention age
Chronology
Production function
Crater

ABSTRACT

We derived crater production functions and chronology functions of Phobos for two scenarios, which likely represent the end-members of its dynamical evolution. Case A assumes that Phobos has been in its current orbit about Mars since its formation. Case B assumes a recent capture of Phobos and the impact history of an average Main Belt Asteroid. We determined the age of an average surface to the west of the Stickney crater and of the interior of the Stickney crater. The results indicate (i) the formation or major collision of Phobos about 4.3 Ga (Case A) or 3.5 Ga (Case B) ago, (ii) the Stickney crater is about 4.2 Ga (Case A) or 2.6 Ga (Case B) old and (iii) grooves probably formed between 3.1 and 3.8 Ga (Case A) or 44 and 340 Ma (Case B). Thus, Stickney seems to be older than the investigated grooves on Phobos.

1. Introduction

Phobos is the inner and larger one of the two natural satellites of Mars. The origin of Phobos is rather uncertain. Its shape, spectral characteristics and density is similar to primitive C-type asteroids (Jones et al., 1990). Therefore, it was proposed that Phobos had its origin in the middle or outer asteroid Main Belt (Veverka et al., 1978). However, it is dynamically difficult to explain how asteroids might permanently be captured into an orbit about Mars. It has, thus alternatively been proposed that Phobos accreted in-situ and has been in orbit about Mars ever since (e.g. Giuranna et al., 2011). In its current orbit inside the classical Roche limit of Mars (e.g. Bills et al., 2005), Phobos is exposed to relatively strong tidal forces which force the satellite into a locked rotation. In conjunction with its small but non-zero eccentricity Phobos also experiences some dynamical friction due to libration oscillations of about 5° about its synchronous position, suggesting the current orbit of Phobos is not stable and it will probably move closer to Mars in the future and might even crash or disintegrate within 30–50 Ma (Burns, 1978). This estimate is considered to be an upper bound by other authors (Bills et al., 2005). However, this also implies that Phobos was in a higher orbit in the past. From tidal dynamics it can be deduced that there is a high probability that Phobos' initial orbit was inside the Mars – synchronous orbit. Otherwise it would have enlarged its orbit due to the tidal interaction similarly to Deimos or the Earth's moon (e.g. Hamelin, 2011). Burns (1978) gives a detailed view of the celestial dynamics of Deimos and Phobos.

Given these uncertainties of the dynamic history of Phobos we developed chronologies for two end-member scenarios for the possible dynamical past of Phobos. One chronology assumes that Phobos has been in its current orbit since its formation (Case A). The other case assumes that Phobos was captured into its current orbit about Mars recently (Case B). The actual past of Phobos is possibly somewhere in between these two extreme cases. The two cases we present here differ somewhat in average impact velocities, impact rates as well as the cratering geometry. Impact velocities are higher in Case A (~8.5 km/s; Case B: ~5 km/s) resulting in larger craters with respect to the same projectile size. Due to projectile–crater scaling relations, the different impact velocities result in slightly different shapes of the crater production function, although both are derived from the lunar case. The different impact velocities and the respective differences in crater scaling in addition to variations in collision frequencies inside the Main Belt vs. collision frequencies at Mars result in formation rates of craters ≥ 1 km about 76 times higher in Case B compared to Case A. Furthermore, for a Main Belt asteroid we would expect an isotropic crater distribution, while Phobos in its current orbit with locked rotation may show a slight asymmetry in crater frequencies between its leading and trailing sides. We test this hypothesis by comparing crater frequencies measured on the leading and trailing

* Correspondence to: Institute of Geological Sciences, Malteserstraße 74-100, Building D, Freie Universität Berlin, 12249 Berlin, Germany. Tel.: +49 30 838 70516; fax: +49 30 838 70539.
E-mail addresses: nico.schmedemann@fu-berlin.de (N. Schmedemann), gregory.michael@fu-berlin.de (G.G. Michael), boris_a_ivanov@mail.ru (B.A. Ivanov), John.Murray@open.ac.uk (J.B. Murray).

http://dx.doi.org/10.1016/j.pss.2014.04.009
0032-0633/

hemisphere of Phobos. If Phobos has been in its current orbit about Mars for a long time i.e. since Mars has formed, it could be expected that its crater size–frequency distribution (SFD) is more similar to the crater production function of Case A, the oldest surface ages may date back as far as the formation of Mars (~4.5 Ga) and we would expect a crater density asymmetry between the leading and trailing hemispheres. If instead Phobos is a recently captured asteroid, it would be expected that its crater distribution follows closer to the Case B crater production function, the oldest surface ages are somewhat younger than Mars' formation and no asymmetry is visible between leading and trailing hemispheres.

Processes which could cause a resurfacing on asteroid-like bodies are for example global and local jolting (Greenberg et al., 1994, 1996), seismic shaking due to neighboring impacts (Richardson et al., 2004, 2005), ejecta blanketing (Cintala et al., 1978) and mass wasting of surface regolith at slopes along the gravitational potential (e.g. Jaumann et al., 2012; Otto et al., 2013), which on small bodies in superposition with tidal and possibly coriolis forces are not necessarily equivalent to topographic slopes (Davis et al., 1981; Hamelin, 2011; Willner et al., 2013). On small bodies such as Phobos seismic shaking may be the dominant process of crater degradation compared to ejecta blanketing (Thomas and Robinson, 2005). Crater degradation induced by seismic shaking e.g. by impacts also appears to be influenced by surface gravity, in a way that it becomes more localized with increasing surface gravity (Richardson, 2013). The low density of Phobos (Willner et al., 2010) as well as the existence of relatively large craters such as Stickney may imply a significantly shattered or fractured interior of Phobos. Considering its low altitude inside the Roche limit of Mars and the non-zero eccentricity of Phobos' orbit, the body might have experienced increasing dynamical stress with decreasing altitude, leading to some kind of tidally induced jolting (e.g. Pollack and Burns, 1977; Soter and Harris, 1977). Such processes could also lead to crater degradation at the surface, if the surface regolith is mobilized. The process forming the grooves on Phobos' surface should have had an impact on the pre-existing cratering record, since it evidently modifies the surface topography. A collection of various groove formation scenarios is given for example by Hamelin (2011). One interesting formation scenario is detailed in Murray et al. (1994) and Murray and Heggie (2014), where ejecta from Mars impact Phobos with specific geometries and statistics that might provide more information on Phobos' history. For instance, they require about 300 craters on Mars with diameters ≥ 100 km in order to explain all the grooves on Phobos. The crater chronology for Mars (Ivanov, 2001) provides a time range of roughly 3.9 Ga in which the most recent of such craters formed, with about 90% being older than 3 Ga. Thus, in this model virtually all grooves formed more than 3 Ga ago. This would also imply that Phobos has been in a locked rotation about Mars since about 3.9 Ga.

Earlier work on the cratering record of Phobos was published by e.g. Thomas and Veverka (1977, 1980). Among their notable results were I) the finding of a crater equilibrium distribution above a crater diameter of 1 km, II) the oldest surface of Phobos is about 4 Ga old, III) the grooves are not recent formations, and IV) Stickney has an age similar to the grooves. In the summary we will compare our results with theirs.

2. Methodology

2.1. Measurements of crater size–frequency distributions

Crater diameters presented in this work were measured on a Phobos basemap based on HRSC imaging data (Wählisch et al., 2010) and a higher resolution HRSC image of Stickney (h3769_004) with a ground resolution of about 8 m/pixel. This image was taken with the super resolution channel of the HRSC camera system (Jaumann et al., 2007) and projected on a spherical reference body with 22.2 km diameter (Willner et al., 2010). For the mapping we used ArcGIS and the CraterTools Plug-in by Kneissl et al. (2011).

2.2. Interpretation of crater distributions

Following the Crater Analysis Techniques Working Group et al. (1979), we fit the crater production function of Phobos to the crater distribution we measured within a counting area, which was outlined to enclose a relatively homogeneous geologic unit using procedures outlined in earlier work (e.g. Baldwin, 1964; Neukum, 1984; Michael and Neukum, 2010). The quoted errors of model ages quantify only the statistical error of the random cratering process but not that of the model calibration. In case an area for crater counting was exposed to resurfacing processes, those should have worked across the whole area homogeneously in order to derive useful crater statistics. Resurfacing processes affect small craters to a higher degree than larger ones, resulting in kinks in the observed crater distribution with shallower slopes towards smaller crater sizes. In a resurfaced crater distribution the end of the resurfacing event can be deduced from the measured distribution, by elimination of craters from the measurement, which were large enough to be not affected by the resurfacing event (Neukum and Hiller, 1981; Hiesinger et al., 2002; Werner, 2005; Hartmann and Werner, 2010; Michael and Neukum, 2010; Fassett et al., 2012; Michael, 2013).

In case an already densely cratered surface is further exposed to meteorite bombardment, for crater sizes observed on Phobos (i.e. diameter $< \sim 10$ km) the crater distribution will reach a state of equilibrium (e.g. Neukum and Dietzel, 1971; Neukum, 1984). Eq. (1) gives the observed lunar equilibrium distribution for small craters (Neukum, 1984).

$$N = 10^{1.1} D^{-2} \quad \left(D\,[\mathrm{km}],\ N\,[\mathrm{km}^{-2}]\right) \tag{1}$$

It may be possible that due to the low surface gravity on Phobos the crater equilibrium is higher density than on the Moon, because of less ejecta blanketing. However, if crater equilibrium is reached, the slope of the observed crater distribution should follow a -2 slope in a cumulative plot (-3 slope in differential plots). If a crater distribution is in production, it should follow a steeper slope around -3 cumulative (-4 differential) as is also observed on Mars for small craters (Neukum and Ivanov, 1994; Werner et al., 2009).

2.3. Randomness analysis

A single geologic unit with uniform resurfacing history is expected to show a spatially random crater distribution. Analysis of the spatial distribution of craters can be used to determine whether the observed population is consistent with being accumulated on a homogeneous geological unit. The degree of clustering or ordering of the measured craters is presented relative to random distributions based on 300 Monte Carlo iterations using the same area geometry as was used for the crater counting (this analysis is described in Michael et al. (2012)). A surface which is appropriate for use in deducing the impactor population or for crater-dating – that is, a unit of homogenous geologic history having accumulated independently-formed impact craters – should show a spatially random crater population. In general, this is also a test for contamination with secondary craters, which often show a clustered distribution (e.g. Werner et al., 2009; Bierhaus et al., 2012). According to Bierhaus et al. (2012) we do

not expect a significant contribution of secondary craters because of the low surface gravity of Phobos.

2.4. Production function

In order to derive surface ages, we calculated the production function of impact craters on Phobos. For this purpose we made use of scaling laws published by Ivanov (2001); Eq. (2). Scaling laws convert projectile diameters into crater diameters and vice-versa. These calculations take into account impact velocities and various physical and material properties of the target and the impacting bodies.

$$\frac{D_t}{D_P\left(\frac{\delta}{\rho}\right)^{0.43}(v\ \sin\ \alpha)^{0.55}} = \frac{1.21}{[(D_{sg}+D_t)g]^{0.28}} \quad (2)$$

Eq. (2): after Ivanov (2001); corrected by Ivanov and Hartmann (2007) and by Ivanov (2008) as his Eq. (8).

Values for variables used in Eq. (2) are given in Table 1. D_t is the diameter of the transient crater. In an additional equation Ivanov (2001) calculates the relation between the diameter of the transient crater and the final crater diameter in the case of complex craters (not existent on Phobos) with diameters larger than the simple to complex transition diameter. Since all craters on Phobos are simple, D_t can be used as crater diameter. D_P is the projectile diameter.

In order to convert the lunar crater production function to Phobos, we use Eq. (2) in the reverse direction first. In this step we calculate the projectile size-frequency distribution from the lunar crater size-frequency distribution. Under the assumption that Phobos has been impacted by the same projectile distribution that impacted the lunar surface, we apply Eq. (2) in the forward direction to Phobos in order to calculate the resulting crater size-frequency distribution for the impact conditions on Phobos. For Cases A and B we only change the mean impact velocity, respectively. The effect of the change in impact velocities on the shape of the production function is shown in Fig. 1 (panel A). This procedure has the advantage that it is independent of modeled projectile distributions, which cannot directly be observed in the Main Belt. Instead we make use of the well investigated lunar cratering record, which provides necessary size distribution information relevant for Phobos.

We estimated the mean impact velocity of projectiles on Phobos for two cases. Case A: Phobos has always been in its current orbit about Mars. Case B: Phobos is a recently captured Main Belt asteroid i.e. Phobos acquired all of its observable craters inside the asteroid Main Belt. In Case A we derived a mean impact velocity of about 8.5 km/s on Phobos from the differences in martian escape velocities at the martian surface and at Phobos' orbit and the previously calculated impact velocities of projectiles at the martian surface of 9.4 km/s (Ivanov, 2008) according to Eq. (3). v_{impP} is the mean impact velocity on Phobos (8.5 km/s), v_{impM} is the mean impact velocity on Mars (9.4 km/s; Ivanov, 2008), v_{escP} is the escape velocity of Mars at Phobos' orbit (3 km/s) and v_{escM} is the escape velocity at the martian surface (5 km/s). Gravitational focusing of Phobos is neglected due to its very low mass.

$$v_{impP} = \sqrt{v_{impM}^2 - v_{escM}^2 + v_{escP}^2} \quad (3)$$

The interaction between the asteroid Main Belt and the inner Solar System implies that the lunar surface could serve as an archetype for crater distributions also for other bodies in the inner Solar System (Ivanov et al., 2002; O'Brien and Greenberg, 2005; Strom et al., 2005; Ivanov, 2008). After application of scaling laws the cratering records of Mars, Phobos as well as the cratering records of Main Belt Asteroids (e.g. Neukum and Ivanov, 1994; Chapman et al., 1996a, 1996b) appear to be highly consistent with the lunar cratering record (Neukum, 1984; Neukum and Ivanov, 1994; Neukum et al., 2001; Hiesinger et al., 2002). Therefore, it is reasonable to assume that the same main impactor source was responsible for the cratering on all of these bodies, namely, the asteroid Main Belt.

2.5. Chronology function

The chronology of the lunar cratering record has been constrained by lunar rock and soil samples from the Apollo and Luna projects (Neukum, 1984; Neukum and Ivanov, 1994). Thus, the Moon gives a constrained relationship between crater frequencies and surface ages. Meteoritic cosmic ray exposure ages show, that meteorites travel from the asteroid Main Belt to Earth quite quickly, with traveling times mostly on the order of a few to some tens of millions of years (e.g. Ivanov, 2001; O'Brien and Greenberg, 2005). Much longer is the half-life time for the exponential decay of the Main Belt projectile population of about 1.40×10^8 a (Neukum, 1984) in the lunar-like chronology. In this setting, any change of flux variations in the Main Belt should reflect in impact rates and thus the chronology functions of the cratering records of the planetary surfaces in the inner Solar System e.g. the Moon. For this reason, the lunar cratering record can be used as general scheme for the chronology function for any inner Solar System body as well as the asteroids themselves but it has to be adapted to the crater formation rate, which is estimated by the impact probability for a particular target body (Ivanov, 2008). Since Phobos is located in orbit about Mars we use the impact probability of asteroids at Mars (Ivanov, 2001) as first order approximation in our Case A.

As already mentioned Phobos shows spectral characteristics common to primitive C-type asteroids (Jones et al., 1990). Therefore, we also derived a chronology function of Phobos for the case that Phobos has been a Main Belt asteroid until it was captured by Mars in recent times (Case B). For this case we used the current average impact probability for Main Belt asteroids (Bottke et al., 1994). The conversion from impact probabilities to impact frequencies is described in O'Brien and Greenberg, 2005. Even in Case B it is appropriate to use a lunar-like chronology, because the lunar chronology is the result of the processes inside the projectile source region, the asteroid Main Belt. Objects in the Main Belt should therefore show a lunar-like chronology as well. A detailed discussion on lunar-like chronologies of Main Belt asteroids is given by Schmedemann et al. (2014).

If Phobos shows an apex-/antapex (leading apex and trailing apex) asymmetry, a respective correction would need to be applied for higher impact rates towards the apex and lower rates towards the antapex. As detailed in Section 3.4 we find no conclusive observational results from our analysis of a cratering asymmetry. Therefore, we do not apply such a correction to our chronology functions. Theoretical analysis of the current orbit of Phobos predicts a factor of about four of cratering asymmetry between the points of apex and antapex of motion. Table 1 gives the parameters we used to derive the crater production function of Phobos from the lunar crater production function for the two cases.

The resulting production and chronology functions of Phobos are shown in Fig. 1. In panel A of Fig. 1 we show the crater production functions. Panel B shows the related lunar-like chronologies of Phobos.

Eq. (4) defines a polynomial of 11th degree for crater production functions following Neukum (1984), Neukum and Ivanov (1994) and Neukum et al. (2001). In this equation N_{cum} is the cumulative crater frequency for craters equal or larger than the

Table 1
Parameters for Converting the Production Function: Parameters for the Moon are taken from Ivanov (2001, 2008). The projectile density is assumed to be 2.5 g/cm³ although 2.7 g/cm³ is published for S-type asteroids (Ivanov, 2008). We chose a slightly lower value because of the likely admixture of lower density C-type asteroids. Simple-to-complex and strength-to-gravity diameters are estimated by a 1/g approach (Pike, 1980), where the lunar values (Ivanov, 2001) are taken as reference.

	Moon	Phobos (Case A)	Phobos asteroid case (Case B)
Target density (g/cm³; ρ)	1.8 (Vasavada et al., 2012)	1.9 (Willner et al., 2010)	1.9 (Willner et al., 2010)
Projectile density (g/cm³; δ)	2.5	2.5	2.5
Impact velocity (km/s; v)	17.5	8.5	5.3
Impact angle (most probable case after Gilbert, 1893; α)	45	45	45
Surface gravity (m/s²; g)	1.62	6×10^{-3} (Willner et al., 2010)	6×10^{-3} (Willner et al., 2010)
Diameter strength to gravity transition (km; D_{sg})	0.3	81	81
Diameter simple to complex (km)	15	4053	4053

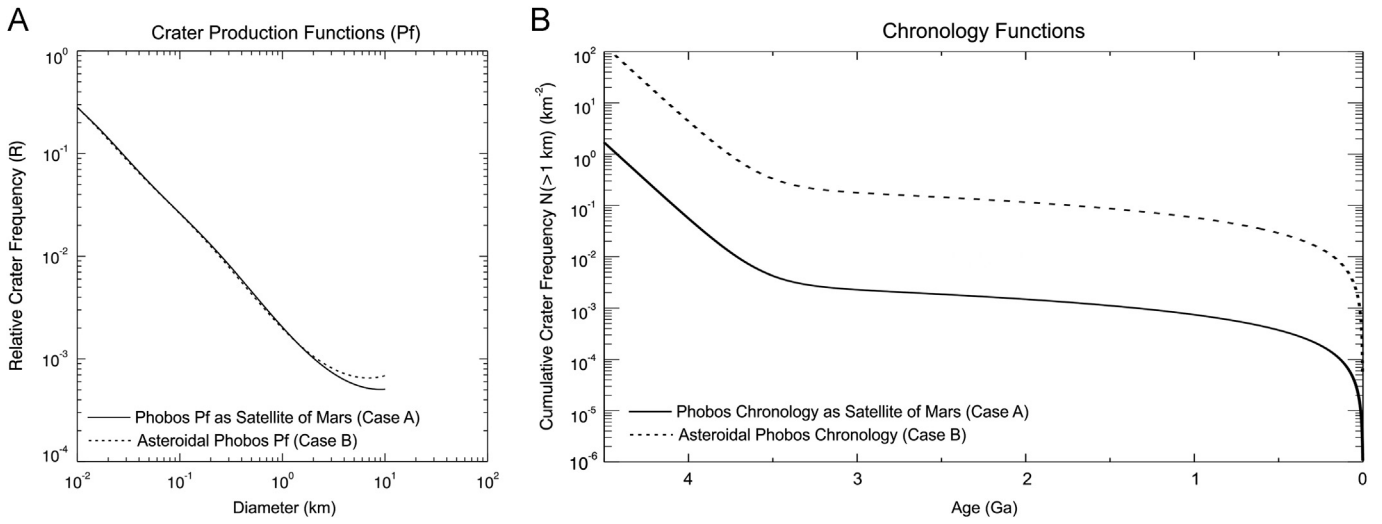

Fig. 1. Crater production and chronology functions for Phobos: Panel A: R-Plots (Crater Analysis Techniques Working Group et al., 1979) of Phobos' crater production functions derived for Case A – always a moon of Mars, and Case B – a recently captured Main Belt asteroid. The functions are normalized to each other at 10 m crater diameter. Thus, they do not reflect the same model age in the respective impact scenarios. Below about 1 km crater size the functions are very similar but at larger sizes the lower impact velocity in the asteroid Main Belt results in a shallower production function. We cut off the functions at 10 km crater size, because there is no larger crater on Phobos. Panel B: Derived lunar-like chronology functions for the two cases of Phobos' evolution based on the respective formation rates of craters ≥ 1 km in diameter in orbit about Mars (0.97 × lunar rate; Case A) and inside the asteroid Main Belt (74 × lunar rate; Case B).

Table 2
Coefficients of Phobos production functions for the Cases A and B.

	Case A	Case B
a_0	−2.5489	−2.8783
a_1	−2.9794	−2.8687
a_2	0.42605	0.53853
a_3	0.32288	0.30803
a_4	−0.030823	−0.048714
a_5	−0.022295	−0.018894
a_6	0.019473	0.00371
a_7	−0.022278	−0.025344
a_8	−0.0085611	−0.0033966
a_9	0.0053854	0.005711
a_{10}	0.00087331	0.0004281
a_{11}	−0.0003887	−0.00036638

crater diameter D and a_x are the coefficients.

$$\log N_{cum} = a_0 + a_1 \log(D) + a_2(\log(D))^2 + \ldots + a_{11}(\log(D))^{11} \quad (4)$$

Table 2 provides the values for the coefficients with respect to the two mentioned cases of Phobos' evolution.

Eq. (5) defines the lunar-like chronology function following Neukum (1984), Neukum and Ivanov (1994) and Neukum et al. (2001). In this equation N_{cum} is the cumulative crater frequency for craters ≥ 1 km, P_{1-3} are the used coefficients and t is the surface age in Ga.

$$N_{cum}(D \geq 1 \text{ km}) = P_1(e^{P_2 t} - 1) + P_3 t \quad (5)$$

Table 3
Coefficients of Phobos' chronology functions for the Cases A and B.

	P1	P2	P3
Case A	5.25×10^{-14}	6.93	8.09×10^{-4}
Case B	4.02×10^{-12}	6.93	6.19×10^{-2}

Table 3 gives the respective values of the derived coefficients for the two cases of Phobos' chronology functions.

3. Results

Fig. 2 gives an overview of the locations and sizes of the used counting areas with respect to the global map presented in an equidistant cylindrical projection.

3.1. Average surface to the west of Stickney

Since Phobos is targeted for observation only when favorable configurations of Mars-observing spacecraft arise, the image

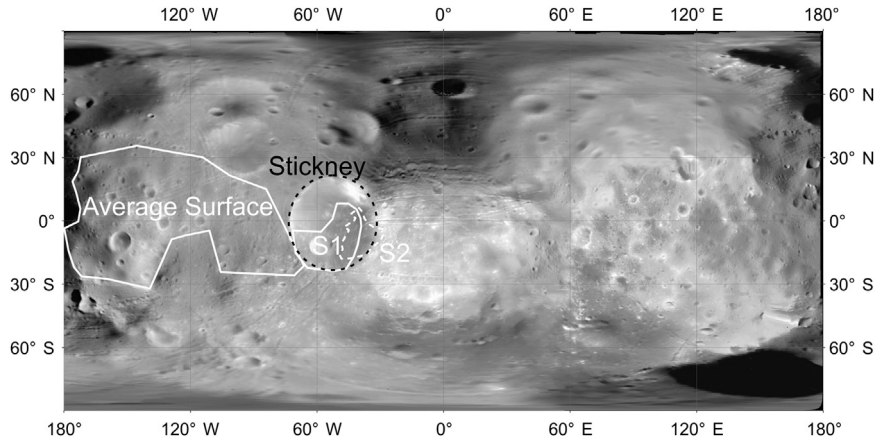

Fig. 2. Area overview: Locations of the used counting areas with respect to the global map given in equidistant cylindrical projection. Areas outlined by white solid polygons were counted on the HRSC basemap (Wählisch et al., 2010). The area S2 is outlined by a white dashed polygon and was counted on a super resolution channel image (h3769_004) of the HRSC camera system.

coverage even with modern HRSC (Wählisch et al., 2010) or HiRISE (McEwen et al., 2010; Thomas et al., 2011) data is uneven. We elected not to measure crater frequencies on a global scale for this analysis, because changing image resolution and geometrically distorted imaging data would have introduced artifacts in the measured crater distribution. Utilizing a Phobos basemap based on HRSC imaging data (Wählisch et al., 2010), we measured crater sizes in what we judged to be a representative average area west of the large crater Stickney to obtain the basic properties of Phobos' cratering record. Although this 177 km² area is affected by at least two sets of grooves cross-cutting each other at about 90° angle, the crater geometries appear relatively unaffected. It appears that the grooves superpose the oldest craters but underlie the youngest craters. Therefore, we expect that groove formation might be visible in the size–frequency distribution data as a resurfacing bump. From a geomorphological point of view it appears that the north–south striking set of grooves is stratigraphically younger than the east–west striking set (Fig. 3, panel A). Fig. 3 (panel B) shows cumulative plots (Crater Analysis Techniques Working Group et al., 1979) of the measured crater size-frequency distribution of Phobos. It is characterized by distinct kinks at about 1.2 km and 500 m crater diameter, which could be interpreted as resurfacing events. The large craters of our measurement (1.5–3.5 km) indicate a surface age of Phobos of $4.27+0.03/-0.04$ Ga (Case A) or $3.50+0.06/-0.1$ Ga (Case B). Craters between 500 m and 1.5 km show frequencies consistent with surface ages of 4.02 ± 0.02 Ga (Case A) or 1.20 ± 0.18 Ga (Case B). Crater frequencies below 500 m crater diameter show surface ages of 3.79 ± 0.02 Ga or 287 ± 27 Ma for the Cases A and B, respectively.

The base age of 4.3 or 3.5 Ga for cases A and B give the times of the last major resurfacing in this area. Thus, the derived age could either reflect the formation of Phobos or indeed a resurfacing of probably global scale. For instance this could be the breakup of the Phobos parent body or other major collisions involving Phobos. It is remarkable, that two resurfacing events are visible in the cratering record of the selected area. As mentioned above, this area also contains two different sets of grooves. It is tempting to draw the conclusion that the resurfacing events are connected to the formation of the two sets of grooves visible in the counting area. If so, the north–south striking set would have been formed about 3.8 Ga (287 Ma – Case B) ago and the east–west striking set about 4 Ga (1.2 Ga – Case B) ago. However, one or both of the observed resurfacing kinks could possibly be related to other processes e.g. impact cratering. Given the close proximity of the Stickney crater (Fig. 2) The formation of Stickney could well be related to a partial resurfacing in the discussed area. Furthermore, the highest measured crater frequencies plot well above the lunar equilibrium for small craters (Fig. 3, panel B). That by itself could indicate a crater distribution close to equilibrium. That would imply that the measured model ages could be lower limits. However, the observed crater distribution is clearly steeper than the -2 slope of the equilibrium distribution and well in agreement with the fitted crater production function. This is an indication that cratering equilibrium is not yet reached and we observe a crater distribution in production. This also implies that the Phobos equilibrium distribution should be located at even higher crater frequencies.

3.2. The interior of Stickney

We measured craters inside Stickney crater in order to determine the age of Stickney. Area S1 contains craters measured on the HRSC basemap (Wählisch et al., 2010). Area S2 contains a separate measurement of craters in the eastern part of Stickney. This part of Stickney is covered by a higher resolution image of the HRSC camera (h3769_0004).

3.2.1. Area S1 on low resolution HRSC basemap

Unfortunately the image quality of the HRSC basemap (Wählisch et al., 2010) varies over the surface area of Stickney significantly. Thus, we took only a fraction of the crater floor of Stickney in order to maintain relatively constant and acceptable image quality. In an updated image mosaic (Wählisch et al., 2013) the discarded area appears to be covered by a landslide, which would not have been included in the counting area anyway, because of its possibly younger formation age. The area (Fig. 4; panel A) is roughly 25 km² in size and it contains the shallow south-western part of the crater rim of Stickney. Therefore, it could be possible that our measurements are affected by some landslide activity close to the crater rim. In the imaging data there are also two sets of grooves visible. The grooved area is also covered by the area S2 in higher resolution. Furthermore, the area contains a comparatively large (~2 km) and fairly fresh crater named Limtoc. The formation of this crater may have caused some level of resurfacing inside Stickney due to seismic shaking. Strong ejecta blanketing is not expected and not obvious, because of the low escape velocity. Thus, it appears to be impossible to date Limtoc crater directly by crater counting on its ejecta blanket, because it

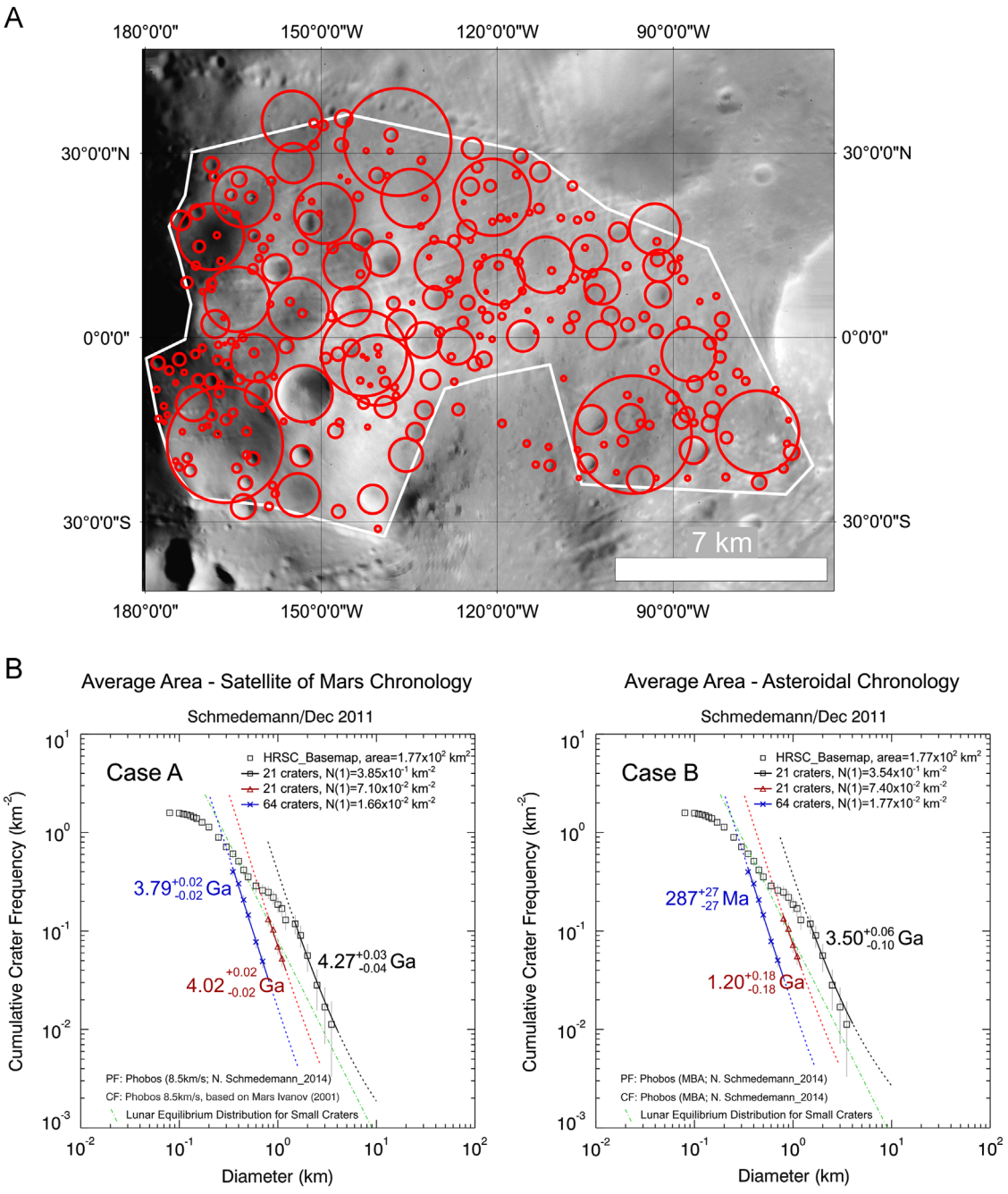

Fig. 3. Map and crater plot of average surface to the west of Stickney: (A) Part of the HRSC basemap of Phobos by Wählisch et al. (2010) in Mercator projection. The counting area and craters are given as white and red outlines, respectively. (B) Measured crater size-frequency distribution of Phobos showing resurfacing kinks at about 1.2 km and 500 m crater diameter. In general the derived crater production functions both seem to fit the data set quite well. The slightly steeper production function in Case A is a little better in agreement with the measured data for the largest crater sizes. For both cases: measured crater distribution – black open squares, older resurfacing corrected crater counts – red triangles, younger resurfacing corrected crater counts – blue crosses, lunar equilibrium distribution for small craters – green dash-dot line. (For interpretation of the references to color in this figure legend, the reader is referred to the web version of this article.)

does not exist. However, from our derived chronology functions, the size of Limtoc and area S1 we could estimate theoretically the time range in which Limtoc possibly did form. For the Case A scenario we find a formation time of roughly 4.2 Ga and 3.3 Ga for Case B.

Similar to Fig. 3 (panel B) in Fig. 4 (panel B) we show the measured cumulative crater size-frequency distribution of area S1 inside the Stickney crater. The crater distribution below about 1 km crater size is flatter than expected from the lunar-like crater SFD. Apart from the roll-over which is caused by resolution issues below about 140 m crater size, this flat distribution features two distinct slopes. These slopes may be indicative of two separate geologic events disturbing the crater distribution by erasing craters more efficiently at small sizes than at large sizes (resurfacing). The kink separating the two slopes is located at about 300 m crater size.

Large craters of our S1 measurement (0.9–1.3 km) indicate a model age for Stickney of $4.15+0.07/-0.13$ Ga (Case A) or $2.64+0.71/-1.50$ Ga (Case B). Craters between 300 m and 900 m show frequencies consistent with surface ages of $3.82+0.03/-0.04$ Ga (Case A) or 341 ± 72 Ma (Case B). Crater frequencies

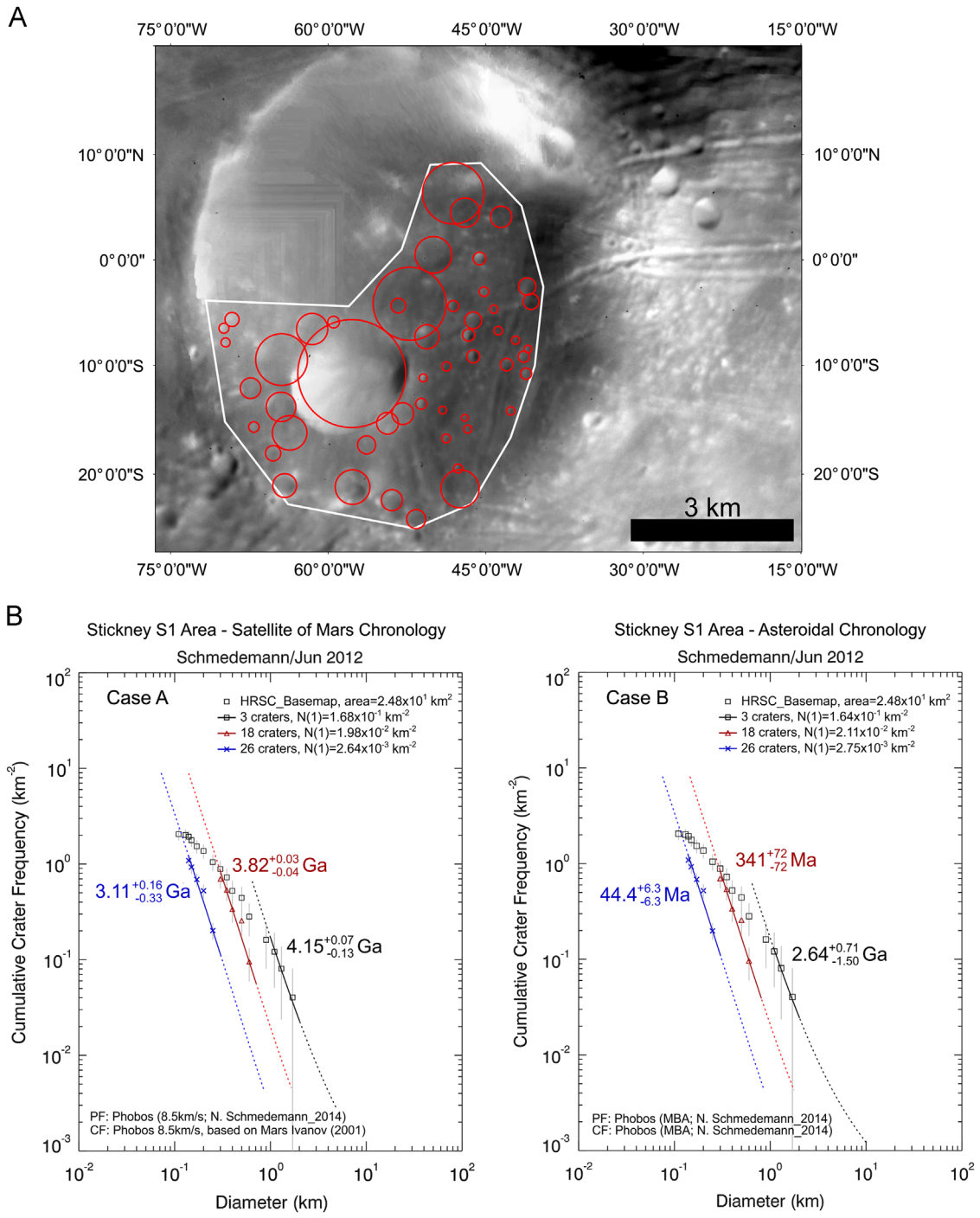

Fig. 4. Map and crater plot of area S1: (A) Stickney crater in the HRSC basemap of Phobos by Wählisch et al. (2010) in Mercator projection. The counting area S1 and craters are given as white and red outlines, respectively. (B) The measured crater size-frequency distribution inside Stickney crater shows kinks at about 900 m and 300 m crater diameter. For both cases: measured crater distribution – black open squares, older resurfacing corrected crater counts – red triangles, younger resurfacing corrected crater counts – blue crosses. (For interpretation of the references to color in this figure legend, the reader is referred to the web version of this article.)

below 300 m crater diameter show surface ages of $3.11+0.16/-0.33$ Ga or 44 ± 6.3 Ma for the Cases A and B respectively.

With about 4.2 Ga (Case A) for the age of the Stickney crater, it is almost as old as the average surface west of Stickney. In the Case B scenario Stickney is nearly 1 Ga younger than the average surface west of Stickney. The age of Stickney from the S1 measurement overlaps slightly within the error bars with the older resurfacing age of $(4.02 \pm 0.02$ Ga$/1.20 \pm 0.18)$ Ga; Case A/Case B) determined from the measurement of the average area east of Stickney. Thus, both ages could possibly indicate the Stickney formation. Although the rim is poorly defined and smoothed over, Stickney appears to show a higher depth to diameter ratio than other similar-sized craters such as Drunlo and Clustril craters. Thus, it appears to be one of the last impacts of such size on Phobos. Our estimated age of the Limtoc crater slightly exceeds that age we measured for the formation of Stickney. Although it is possible that Limtoc formed at any later point in time, it probably formed shortly after Stickney when almost no other craters still visible today were present on the floor of Stickney. It may also be possible that the formation of Limtoc

erased the preexisting cratering record inside Stickney. In that case the highest age of this area is the formation time of Limtoc. This possibility appears less likely than a formation of Limtoc shortly after Stickney with both craters of similar age.

The two resurfacing events are not quite well constrained from crater counts. If these two resurfacings are not caused by issues due to the quality of the images, they could be indicating the age of the large, sharp rimmed Limtoc crater in the counting area, the age of the grooves inside Stickney or may simply be caused by slumping events on the slope of Stickney. Area S2 is more suited to resolve these younger ages, because of the higher image resolution and therefore also better determination of small crater frequencies. Fig. 4 (panel A) shows a Mercator projection of the measurement area S1 together with the measured craters projected onto the HRSC basemap (Wählisch et al., 2010).

3.2.2. *Area S2 on high resolution HRSC image h3769_0004*

The HRSC image h3769_0004 shows only the eastern part of the Stickney crater (Fig. 5, panel A). Its resolution is about 10 m per pixel. The counting area is roughly 10 km² in size and it includes a part of the eastern crater rim of Stickney. This part of the rim is topographically higher than the southern part and therefore this measurement might also be even more affected by landslides on the slope of the crater rim. However, its current dynamic height is relatively low (Willner et al., 2013), which would imply a lower probability for mass wasting events. This counting area overlaps with area S1 and it contains two sets of grooves crossing each other inside the counting area. Based on a morphologic interpretation it appears that the north–south striking set of grooves is older than the east–west striking solitary groove, because the north–south grooves do not continue through the east–west groove. There is morphologic evidence that both sets of grooves superimpose the ~2 km Limtoc crater inside Stickney. Thus, Limtoc crater might pre-date both groove formation events, which would be consistent with the idea that Limtoc formed immediately after Stickney. The Limtoc impact event might have caused landslides on the crater walls of Stickney. This probably happened on the western crater wall of Stickney, where landslides of

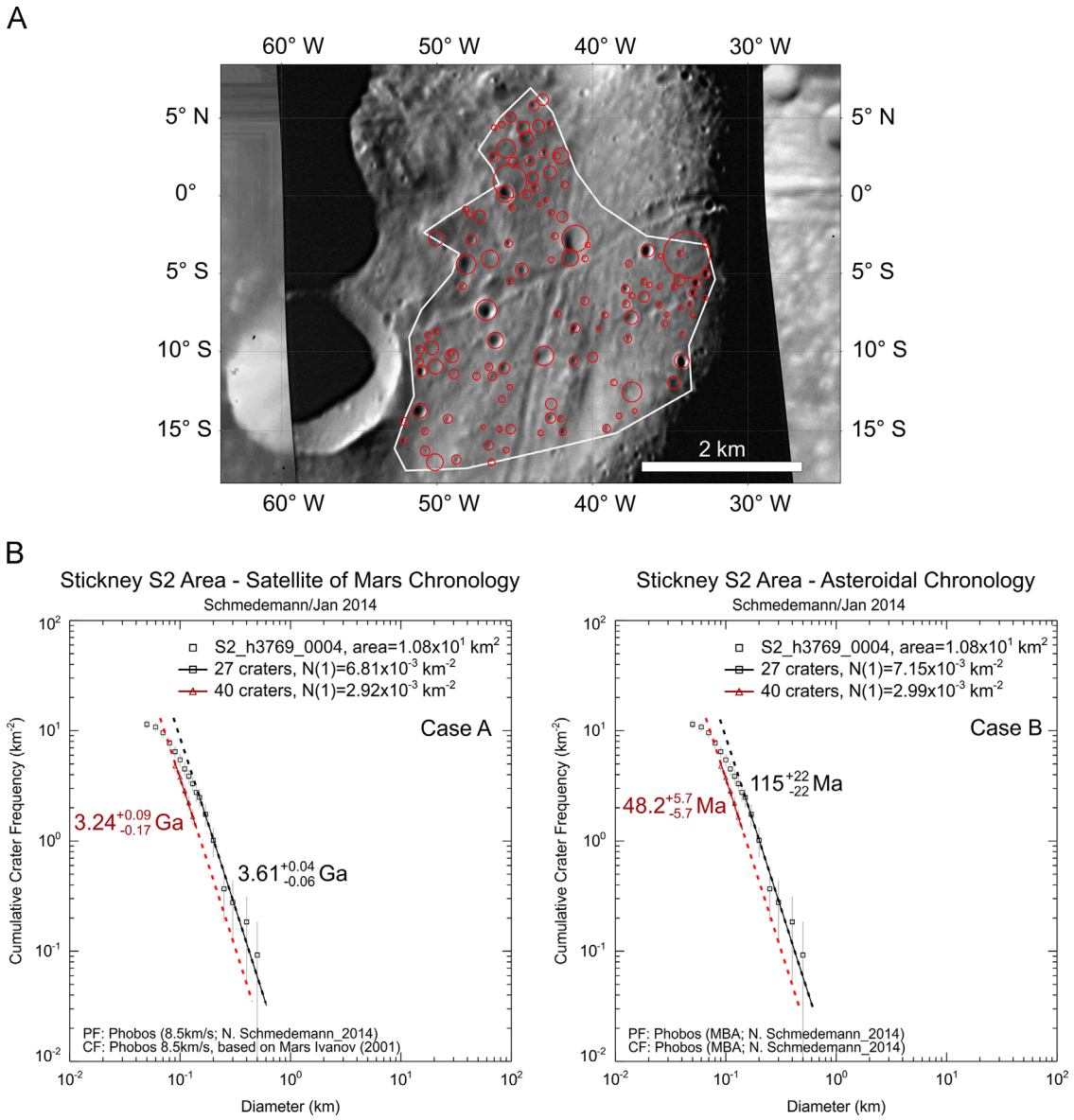

Fig. 5. Map and crater plot of area S2: (A) Eastern part of Stickney crater in the HRSC image "h3769_0004" in Mercator projection. The counting area S2 and craters are given as white and red outlines, respectively. (B) For both cases: measured crater distribution – black open squares, resurfacing corrected crater counts – red triangles. (For interpretation of the references to color in this figure legend, the reader is referred to the web version of this article.)

possibly different ages are apparent on HiRISE (McEwen et al., 2010) imaging data (http://static.uahirise.org/images/2008/details/phobos/PSP_007769_9010_IRB.jpg; 23. JAN 2014). The grooves in our counting area, which are located on the eastern crater wall of Stickney do not show obvious degradation by landslides. Thus, large landslides probably did not occur on the eastern crater wall of Stickney.

Fig. 5 (panel B) shows a cumulative plot of the measurement taken in area S2. Because of the higher resolution imaging data the crater plot shows more detail for small craters but lacks larger craters due to the limited area. We identified a possible resurfacing for crater sizes smaller than ~190 m. For Cases A and B this resurfacing ended about $3.24+0.09/-0.17$ Ga or 48 ± 5.7 Ma ago. Within the error bars these ages are in agreement with the younger resurfacing event found in area S1. The model age for craters >190 m of this measurement is $3.61+0.04/-0.06$ Ga or 115 ± 22 Ma for Cases A and B. Under consideration of resurfacing ages of area S1 the mentioned morphology-based stratigraphic order of the Limtoc crater and the grooves may suggest an age of about 3.6–3.8 Ga (0.12–0.34 Ga, Case B) for the formation of the north–south striking set of grooves. The younger resurfacing age indicates the formation of the east–west striking groove about 3.1–3.2 Ga or 44–48 Ma ago for Cases A and B, respectively.

3.3. Spatial randomness analysis

Fig. 6 shows the distribution of crater size dependent clustering effects of measured craters in the three mentioned areas. Following the method of Michael et al. (2012) we examine the value of a clustering measure (here we use the standard deviation of adjacent area (SDAA)) with respect to a series of random configurations of craters generated over the same counting area. Strong deviations of the measured value from the random series suggest that the counting area is not homogeneous, and likely incorporates regions of varying age or geologic history. In this work we consider that measures which fall within $\pm 3\sigma$ of the mean for the random series are consistent with being random and are thus valid populations to use for crater dating.

The average area west of Stickney shows a random spatial crater distribution for crater sizes >500 m. Below 500 m the craters are slightly clustered. This slight clustering could be caused by variations in the illumination conditions but it is also possible that the groove formation or seismic shaking due to the Stickney impact may have influenced the spatial distribution of the smaller craters. Area S1 is characterized by a random crater distribution for crater sizes >250 m. Craters smaller 250 m are slightly clustered. The reason for this clustering could be the changing image quality across the counting area. Thus, smaller craters are harder to recognize in lower quality parts of the image. Area S2 shows a random crater distribution for all craters. As observed in the other areas craters <125 m show a tendency for slight clustering. Besides changing illumination conditions it might be possible the slight clustering is a real geomorphologic effect possibly caused by some resurfacing process which did not act uniformly over the counting area. The SDAA randomness test is not possible if there are fewer than three craters in the diameter bin. This is often the case for the largest one or two measured crater size bins.

3.4. Crater density asymmetry at apex and antapex points of orbital motion

It may be expected that for a body which has long been in locked orbit around Mars, there may be an asymmetry between the density of craters at the apex/antapex points of orbital motion.

Following Zahnle et al. (2001), using circular counting areas within 30° of the along-orbit axis (~11.6 km diameter) we measured a density ratio of 0.6 for this effect. Surprisingly, the higher crater frequency is determined in the area at the antapex. The map in Fig. 7 (panel A) shows the counting areas and mapped craters for this analysis. Fig. 7 (panel B) shows the respective crater plots. It is apparent that we are dealing with small number statistics. Although we used fractional crater counting (Platz et al., 2013) in order to improve crater statistics we are able to fit only 3 or 4 crater size bins in each measurement, but the error bars overlap. Thus, we cannot confirm the existence of a cratering asymmetry between the apex and antapex of motion on Phobos. We analyzed the crater density only for relatively large diameters, which give insight to the early cratering history. With respect to the described two scenarios the non-existence of an apex-/antapex asymmetry could mean for Case A that Phobos was not or not permanently locked in its current position. Major impacts may have changed Phobos' orientation from time to time during its early history. For the Case B scenario all craters formed inside the Main Belt and a cratering asymmetry is not expected, possibly consistent with our observation. Small craters could give insight to

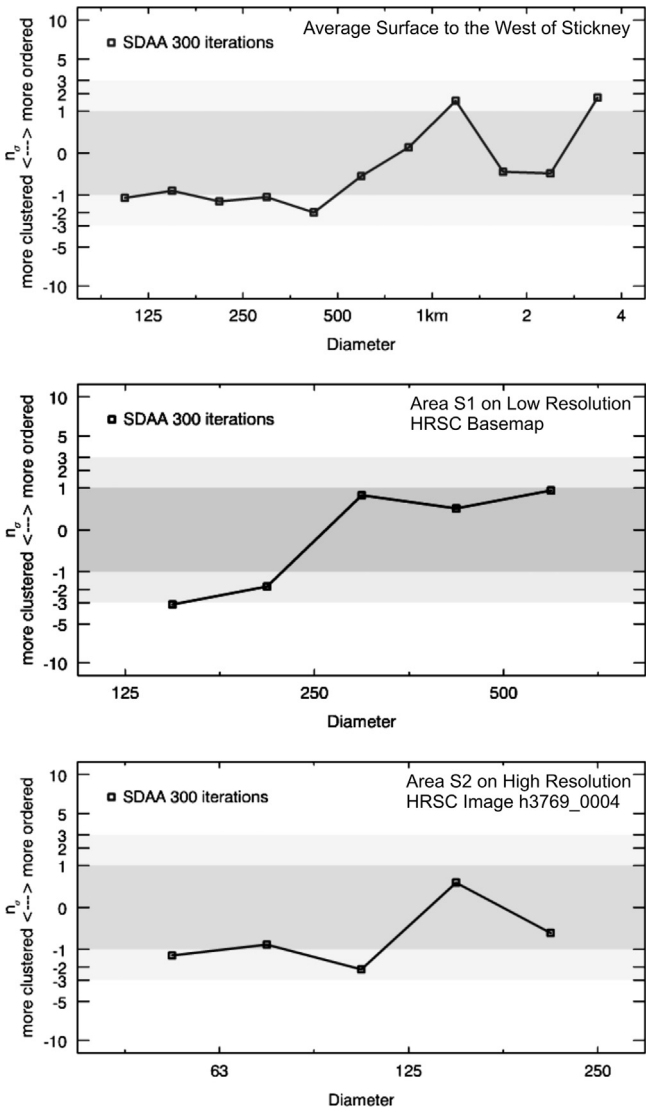

Fig. 6. Randomness Analysis: Value of SDAA (standard deviation of adjacent area) clustering measure for three crater counts with respect to a series of random configurations of craters generated over an equivalent counting area (Michael et al., 2012). The analysis is made separately for craters of different sizes, the population being split into bins with a $\sqrt{2}$ diameter spacing. The dark gray band represents the range $\pm 1\sigma$ from the mean; the light gray bands, to $\pm 3\sigma$.

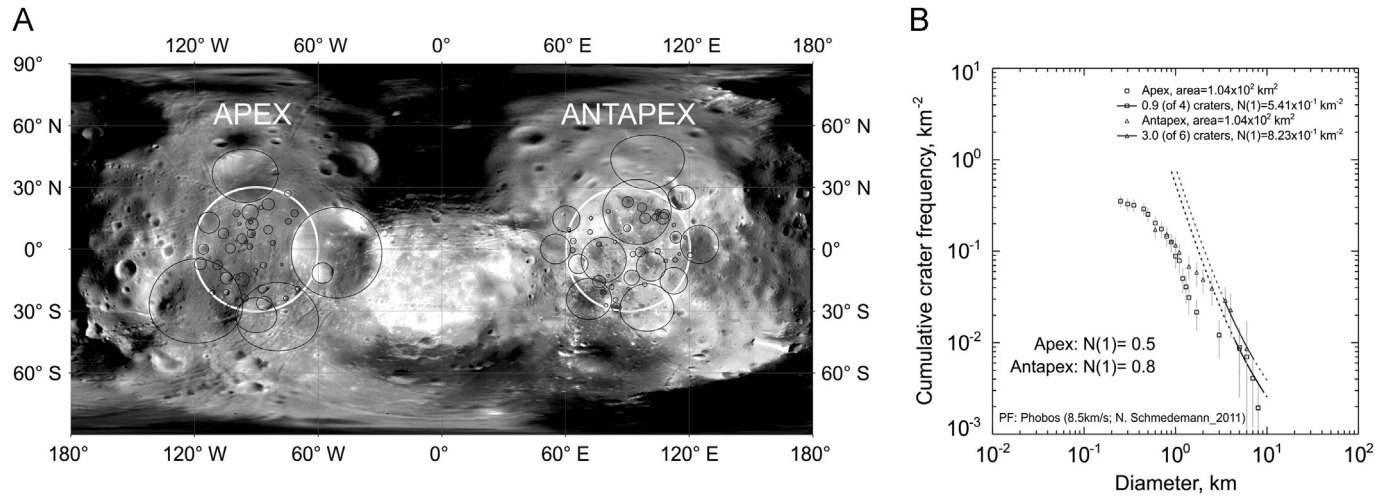

Fig. 7. Apex/Antapex Asymmetry Measurement: (A) HRSC basemap (Wählisch et al., 2010) in equatorial equidistant projection with apex and antapex counting areas (white circles). Apex and antapex areas are defined as circles with 30 degree radius on the surface of Phobos around the apex (longitude: −90°, latitude: 0°) and antapex (longitude: 90°, latitude: 0°) point of motion. Very small craters are not mapped, because they are affected by resurfacing. (B) Fit of the production function (Case A) to the measured crater distributions. The extrapolated value of the cumulative crater frequencies at 1 km crater size are 0.5 km^{-2} for the leading side (apex) and 0.8 km^{-2} for the trailing side (antapex). Thus, we measure a ratio in crater frequencies of a factor of about 0.6 ± 0.8 between the leading and trailing side of Phobos.

the most recent cratering history of Phobos. We did not analyze smaller crater sizes for apex/antapex asymmetry, because at least the apex area shows multiple resurfacing events. Thus, a comparison to the antapex area is not trivial.

Eq. (6) gives a theoretical estimation of the expected current ratio of the cratering rate (γ) between the apex and the antapex of motion of Phobos following Horedt and Neukum (1984), Zahnle et al. (2001) and Morota et al. (2008).

$$\gamma = \left(\frac{1 + \frac{v_{orb}}{\sqrt{2v_{orb}^2 + v_\infty^2}} \cos\beta}{1 - \frac{v_{orb}}{\sqrt{2v_{orb}^2 + v_\infty^2}} \cos\beta} \right)^{2.742} \quad (6)$$

The current orbital velocity (v_{orb}) of Phobos is about 2.14 km/s. The projectile velocity at infinity (v_∞) follows from Eq. (1) by neglecting the term of Mars' escape velocity at Phobos' orbit and has a value of about 8 km/s. For β we use values $\leq 30°$. Thus we expect a cratering ratio between the points of apex and antapex of Phobos' motion of about 4.

4. Summary

We calibrate the lunar crater production function for Phobos' conditions based on dynamical estimates for an impact history of Phobos in its current orbit about Mars (Case A) and for an asteroidal impact history which implies that Phobos was captured into its current orbit (Case B) relatively recently (less than ~40 Ma ago). These two scenarios also require respective chronologies which are based on a lunar-like chronology, assuming the same time dependent behavior in impact rates. The chronology of Case A is based on impact rates on Mars (Ivanov, 2001), while the Case B chronology is based on the current average impact probability between Main Belt asteroids (Bottke et al., 1994).

The crater equilibrium reported by Thomas and Veverka (1977) is not apparent in our measurements for the oldest surface we measured (average area west of Stickney). Instead we find a crater distribution in production, although already above the lunar equilibrium distribution for small craters.

Our results for the Case A scenario are roughly consistent with Thomas and Veverka (1980), while the Case B scenario differs more strongly. I – TV(1980): The oldest surface is about 4 Ga old. We found an age of ~4.3 Ga in our Case A scenario and ~3.5 Ga in Case B. II – TV(1980): The grooves are not recent formations. We found ages of 3.1–3.8/44–340 Ma (notation: Case A/Case B) in our areas, which could be linked to groove formation on Phobos. Thus, in our Case B the grooves are recent formations, while they are ancient in Case A. Causes other than groove formation for the resurfacing ages are also possible. ~4.0/1.2 Ga is a resurfacing age in the area to the west of Stickney. Within the error bars it is the same age we derive for Stickney formation in area S1 (~4.2/2.64 Ga). Given the close spatial neighborhood it is more reasonable to relate both ages to the formation of Stickney than to introduce a groove formation event at the average area at ~4.0/1.2 Ga. The younger resurfacing age (~3.8 Ga/~290 Ma) from the average area to the west of Stickney and the older resurfacing age in area S1 (~3.8 Ga/~340 Ma) are the same within the error bars and the older age in area S2 (~3.6 Ga/~120 Ma) is similar but not the same within the error bars. Possibly all these ages (~3.6 to ~3.8 Ga/~120 to ~340 Ma) might date just one event of groove formation. The youngest ages found in areas S1 and S2 3.1–3.2 Ga/44–48 Ma might date a younger groove formation event. Based on morphologic investigations Limtoc appears stratigraphically older then both sets of grooves inside Stickney (Murray et al., 1994; Murray and Heggie, 2014). From theoretical estimation for the formation of Limtoc it appears possible that it formed immediately after Stickney and thus its formation is not recorded as resurfacing event in the area S1. Orientation angle and stratigraphic superposition of the east–west striking groove may imply at least two separate groove formation events possibly resolved by our measurements. III – TV(1980): Stickney has a similar age to the grooves. We found an age of about 4–4.2/1.2–2.64 Ga (notation: Case A/Case B) for Stickney. For Case A this is slightly older than the formation of grooves at about 3.1–3.8/0.44–0.34 Ga. For Case B the difference is more than 1 Ga. Thus, if Stickney is older than the grooves and even multiple sets of grooves exist inside Stickney, which probably formed not together in one event; it appears that Stickney is probably not responsible for groove formation on Phobos. Grooves and troughs have been found on asteroids such as (433) Eros (Buczkowski et al., 2008), (21) Lutetia (Thomas et al., 2012) and (4) Vesta (Jaumann et al., 2012). Thomas et al. (2012) give a broad discussion on the quite diverse pattern of linear features on (21) Lutetia connected with related formation processes.

In addition to the statistical errors, the estimated absolute ages are also affected by other uncertainties. For example in the case of

the average area west of Stickney the measured area is larger than the morphological extent of the grooves and it might be possible that the resurfacing acted unequally over the counting area at both events. However, such unevenness was not detected by the randomness analysis.

Unfortunately the imaging data we used in this work is not sufficient to do meaningful measurements on a global scale to characterize the crater distribution on Phobos in more detail. Although we cannot prove or disprove an apex/antapex asymmetry, it is possible that a cratering anisotropy could have an effect on any age determination based on the cratering record of Phobos. An apex-/antapex anisotropy could be an indication that Phobos has been in a locked rotation about Mars for a long time and that Phobos was not captured recently. A shielding effect by Mars causing higher cratering rates on the far-side could not be detected in this work. The only indication that our Case A is more probable than Case B is our measurement of the average area west of Stickney. The slight difference in the crater production function between our Cases A and B is best visible at large crater sizes. The mentioned area contains such craters and at the largest crater sizes the crater production function for Case A fits slightly better to our measurement than the production function of Case B (Fig. 3). However, Bottke et al. (1994) estimated for the similar-sized Main Belt asteroid Gaspra a collisional lifetime of roughly 500 Ma. Based on this estimate we may speculate that Phobos was not a member of the asteroid Main Belt at least during the last ~500 Ma. Thus, if Phobos is a captured asteroid, as its spectral characteristic implies, it likely has been captured very early in the Solar System history, when the asteroid flux at Mars was much higher than during the last 3.5 Ga.

This is also supported by the work of Murray et al. (1994) and Murray and Heggie (2014). Based on their model the number and geometry of the groove families would require that Phobos is in a locked rotation about Mars since ~3.9 Ga. If it resided longer in such a configuration, we might see more sets of grooves. Thus, ~3.9 Ga might also be the time at which Phobos could have been captured, if it is a captured asteroid.

In case farther dispersed secondary projectiles from Mars impacted Phobos in significant numbers, age determination by crater counting could become meaningless due to the secondary contamination. We do not think that this is an issue, because large numbers of secondaries would have been manifested as a steep crater distribution in our measurements, which was not observed.

The results of this work are based on rather inhomogeneous imaging data. Once a more homogeneous imaging atlas of Phobos is available (e.g. Wählisch et al., 2013), the presented results could be refined.

Acknowledgment

This work has been supported by the German Space Agency (DLR) on behalf of the Federal Ministry for Economic Affairs and Energy, Germany, Grant 50QM1301 (GM). We thank the reviewers for their constructive comments.

References

Baldwin, R.B., 1964. Lunar crater counts. Astron. J. 69, 377.
Bierhaus, E.B., Dones, L., Alvarellos, J.L., Zahnle, K., 2012. The role of ejecta in the small crater populations on the mid-sized saturnian satellites. Icarus 218, 602–621.
Bills, B.G., Neumann, G.A., Smith, D.E., Zuber, M.T., 2005. Improved estimate of tidal dissipation within Mars from MOLA observations of the shadow of Phobos. J. Geophys. Res. 110, E07004.
Bottke, W.F., Nolan, M.C., Greenberg, R., Kolvoord, R.A., 1994. Velocity distributions among colliding asteroids. Icarus 107, 255–268.
Buczkowski, D.L., Barnouin-Jha, O.S., Prockter, L.M., 2008. 433 Eros lineaments: global mapping and analysis. Icarus 193, 39–52.
Burns, J.A., 1978. The dynamical evolution and origin of the Martian moons. Vistas Astron. 22 (Part 2), 193–210.
Chapman, C.R., Ryan, E.V., Merline, W.J., Neukum, G., Wagner, R., Thomas, P.C., Veverka, J., Sullivan, R.J., 1996a. Cratering on Ida. Icarus 120, 77–86.
Chapman, C.R., Veverka, J., Belton, M.J.S., Neukum, G., Morrison, D., 1996b. Cratering on Gaspra. Icarus 120, 231–245.
Cintala, M.J., Head, J.W., Veverka, J., 1978. Characteristics of the cratering process on small satellites and asteroids. In: Proceedings of the 9th Lunar and Planetary Science Conference (A79-39253 16-91), Houston, Tex., March 13–17, 1978. New York, Pergamon Press, Inc., pp. 3803–3830.
Crater Analysis Techniques Working GroupArvidson, R.E., Boyce, J., Chapman, C., Cintala, M., Fulchignoni, M., Moore, H., Neukum, G., Schultz, P., Soderblom, L., Strom, R., Woronow, A., Young, R., 1979. Standard techniques for presentation and analysis of crater size-frequency data. Icarus 37 (1979), 467–474.
Davis, D.R., Housen, K.R., Greenberg, R., 1981. The unusual dynamical environment of Phobos and Deimos. Icarus 47, 220–233.
Fassett, C.I., Head, J.W., Kadish, S.J., Mazarico, E., Neumann, G.A., Smith, D.E., Zuber, M.T., 2012. Lunar impact basins: Stratigraphy, sequence and ages from superposed impact crater populations measured from lunar orbiter laser altimeter (LOLA) data. J. Geophys. Res. (Planets), 117.
Giuranna, M., Roush, T.L., Duxbury, T., Hogan, R.C., Carli, C., Geminale, A., Formisano, V., 2011. Compositional interpretation of PFS/MEx and TES/MGS thermal infrared spectra of Phobos. Planet. Sp. Sci. 59, 1308–1325.
Greenberg, R., Bottke, W.F., Nolan, M., Geissler, P., Petit, J.-M., Durda, D.D., Asphaug, E., Head, J., 1996. Collisional and dynamical history of Ida. Icarus 120, 106–118.
Greenberg, R., Nolan, M.C., Bottke Jr, W.F., Kolvoord, R.A., Veverka, J., 1994. Collisional history of Gaspra. Icarus 107, 84–97.
Hamelin, M., 2011. Motion of blocks on the surface of Phobos: new constraints for the formation of grooves. Planet. Sp. Sci. 59, 1293–1307.
Hartmann, W.K., Werner, S.C., 2010. Martian Cratering 10. Progress in use of crater counts to interpret geological processes: Examples from two debris aprons. Earth Planet. Sci. Lett. 294, 230–237.
Hiesinger, H., Head, J.W., Wolf, U., Jaumann, R., Neukum, G., 2002. Lunar mare basalt flow units: thicknesses determined from crater size-frequency distributions. Geophys. Res. Lett. 29, 81–89 (CiteID 1248, DOI 1210).
Horedt, G.P., Neukum, G., 1984. Cratering rate over the surface of a synchronous satellite. Icarus 60, 710–717.
Ivanov, B., 2008. Size-frequency distribution of asteroids and impact craters. In: Adushkin, V.V., Nemchinov, I.V. (Eds.), Estimates of Impact Rate Catastrophic Events Caused by Cosmic Objects. Springer, Berlin, ISBN: 978-1-4020-6451-7, p. 91.
Ivanov, B.A., 2001. Mars/Moon cratering rate ratio estimates. Sp. Sci. Rev. 96, 87–104.
Ivanov, B.A., Hartmann, W.K., 2007. 10.06 – Exogenic dynamics, cratering and surface ages. In: Gerald, S. (Ed.), Treatise on Geophysics. Elsevier, Amsterdam, pp. 207–242.
Ivanov, B.A., Neukum, G., Bottke Jr., W.F., Hartmann, W.K., 2002. In: Asteroids III, W. F., Bottke Jr., A., Cellino, P., Paolicchi, Binzel, R.P. (Eds.), The Comparison of Size-Frequency Distributions of Impact Craters and Asteroids and the Planetary Cratering Rate. University of Arizona Press, Tucson, pp. 89–101.
Jaumann, R., Neukum, G., Behnke, T., Duxbury, T.C., Eichentopf, K., Flohrer, J., Gasselt, S.v., Giese, B., Gwinner, K., Hauber, E., Hoffmann, H., Hoffmeister, A., Kohler, U., Matz, K.D., McCord, T.B., Mertens, V., Oberst, J., Pischel, R., Reiss, D., Ress, E., Roatsch, T., Saiger, P., Scholten, F., Schwarz, G., Stephan, K., Wählisch, M., 2007. The high-resolution stereo camera (HRSC) experiment on Mars express: instrument aspects and experiment conduct from interplanetary cruise through the nominal mission. Planet. Sp. Sci. 55, 928–952.
Jaumann, R., Williams, D.A., Buczkowski, D.L., Yingst, R.A., Preusker, F., Hiesinger, H., Schmedemann, N., Kneissl, T., Vincent, J.B., Blewett, D.T., Buratti, B.J., Carsenty, U., Denevi, B.W., De Sanctis, M.C., Garry, W.B., Keller, H.U., Kersten, E., Krohn, K., Li, J.Y., Marchi, S., Matz, K.D., McCord, T.B., McSween, H.Y., Mest, S.C., Mittlefehldt, D.W., Mottola, S., Nathues, A., Neukum, G., O'Brien, D.P., Pieters, C.M., Prettyman, T.H., Raymond, C.A., Roatsch, T., Russell, C.T., Schenk, P., Schmidt, B. E., Scholten, F., Stephan, K., Sykes, M.V., Tricarico, P., Wagner, R., Zuber, M.T., Sierks, H., 2012. Vesta's shape and morphology. Science 336, 687.
Jones, T.D., Lebofsky, L.A., Lewis, J.S., Marley, M.S., 1990. The composition and origin of the C, P, and D asteroids: water as a tracer of thermal evolution in the outer belt. Icarus 88, 172–192.
Kneissl, T., van Gasselt, S., Neukum, G., 2011. Map-projection-independent crater size-frequency determination in GIS environments – new software tool for ArcGIS. Planet. Sp. Sci. 59, 1243–1254.
McEwen, A.S., Banks, M.E., Baugh, N., Becker, K., Boyd, A., Bergstrom, J.W., Beyer, R.A., Bortolini, E., Bridges, N.T., Byrne, S., Castalia, B., Chuang, F.C., Crumpler, L.S., Daubar, I., Davatzes, A.K., Deardorff, D.G., DeJong, A., Alan Delamere, W., Dobrea, E.N., Dundas, C.M., Eliason, E.M., Espinoza, Y., Fennema, A., Fishbaugh, K.E., Forrester, T., Geissler, P.E., Grant, J.A., Griffes, J.L., Grotzinger, J.P., Gulick, V.C., Hansen, C.J., Herkenhoff, K.E., Heyd, R., Jaeger, W.L., Jones, D., Kanefsky, B., Keszthelyi, L., King, R., Kirk, R.L., Kolb, K.J., Lasco, J., Lefort, A., Leis, R., Lewis, K.W., Martinez-Alonso, S., Mattson, S., McArthur, G., Mellon, M.T., Metz, J.M., Milazzo, M.P., Milliken, R.E., Motazedian, T., Okubo, C.H., Ortiz, A., Philippoff, A.J., Plassmann, J., Polit, A., Russell, P.S., Schaller, C., Searls, M.L., Spriggs, T., Squyres, S.W., Tarr, S., Thomas, N., Thomson, B.J., Tornabene, L.L., Van Houten, C., Verba, C., Weitz, C.M., Wray, J.J., 2010. The high resolution imaging science experiment (HiRISE) during MRO's primary science phase (PSP). Icarus 205, 2–37.

Michael, G.G., 2013. Planetary surface dating from crater size–frequency distribution measurements: multiple resurfacing episodes and differential isochron fitting. Icarus 226, 885–890.
Michael, G.G., Neukum, G., 2010. Planetary surface dating from crater size-frequency distribution measurements: partial resurfacing events and statistical age uncertainty. Earth Planet. Sci. Lett. 294, 223–229.
Michael, G.G., Platz, T., Kneissl, T., Schmedemann, N., 2012. Planetary surface dating from crater size–frequency distribution measurements: spatial randomness and clustering. Icarus 218, 169–177.
Morota, T., Haruyama, J.I., Honda, C., Yokota, Y., Ohtake, M., Furumoto, M., 2008. Lunar apex–antapex cratering asymmetry as an impactor recorder in the Earth–Moon system. Adv. Sp. Res. 42, 285–288.
Murray, J.B., Heggie, D.C., 2014. Character and origin of Phobos' grooves. Planet. Sp. Sci. 102, 119–143, http://dx.doi.org/10.1016/j.pss.2014.03.001.
Murray, J.B., Rothery, D.A., Thornhill, G.D., Muller, J.P., Iliffe, J.C., Day, T., Cook, A.C., 1994. The origin of Phobos' grooves and crater chains. Planet. Sp. Sci. 42, 519–526.
Neukum, G., 1984. Meteorite Bombardment and Dating of Planetary Surfaces. Publication: Thesis – February 1983, National Aeronautics and Space Administration, Washington, DC. Transl. into English of "Meteoritenbombardement und Datierung Planetarer Oberflaechen" Munich, February 1983, pp. 1–186.
Neukum, G., Dietzel, H., 1971. On the development of the crater population on the moon with time under meteoroid and solar wind bombardment. Earth Planet. Sci. Lett. 12, 59–66.
Neukum, G., Hiller, K., 1981. Martian ages. J. Geophys. Res. 86, 3097–3121.
Neukum, G., Ivanov, B.A., 1994. Crater size distributions and impact probabilities on earth from lunar, terrestrial-planet, and asteroid cratering data. In: Gehrels, Tom, Matthews, M.S., Schumann, A. (Eds.), Hazards due to comets and asteroids. Space Science Series, 1994. Published by University of Arizona Press, Tucson, AZ, p. 359.
Neukum, G., Ivanov, B.A., Hartmann, W.K., 2001. Cratering records in the inner solar system in relation to the lunar reference system. Sp. Sci. Rev. 96, 55–86.
O'Brien, D.P., Greenberg, R., 2005. The collisional and dynamical evolution of the main-belt and NEA size distributions. Icarus 178, 179–212.
Otto, K.A., Jaumann, R., Krohn, K., Matz, K.-D., Preusker, F., Roatsch, T., Schenk, P., Scholten, F., Stephan, K., Raymond, C.A., Russell, C.T., 2013. Mass-wasting features and processes in Vesta's south polar basin Rheasilvia. J. Geophys. Res.: Planets.
Pike, R.J., 1980. Formation of complex impact craters: Evidence from Mars and other planets. Icarus 43, 1–19.
Platz, T., Michael, G., Tanaka, K.L., Skinner Jr, J.A., Fortezzo, C.M., 2013. Crater-based dating of geological units on Mars: methods and application for the new global geological map. Icarus 225, 806–827.
Pollack, J.B., Burns, J.A., 1977. An Origin by Capture for the Martian Satellites? Bull. Am. Astron. Soc. 9, 518.
Richardson, J.E., 2013. Three-dimensional modeling of crater degradation via the effects of impact induced seismic shaking, with comparison to crater count data. LPI Contributions, vol. 1719; p. 2397.
Richardson, J.E., Melosh, H.J., Greenberg, R., 2004. Impact-induced seismic activity on asteroid 433 Eros: a surface modification process. Science 306, 1526–1529.
Richardson Jr, J.E., Melosh, H.J., Greenberg, R.J., O'Brien, D.P., 2005. The global effects of impact-induced seismic activity on fractured asteroid surface morphology. Icarus 179, 325–349.
Schmedemann, et al., 2014. The cratering record, chronology and surface ages of (4) Vesta in comparison to smaller asteroids and ages of HED meteorites. Planet. Sp. Sci. 10.1016/j.pss.2014.04.004.
Soter, S., Harris, A., 1977. Are striations on Phobos evidence for tidal stress? Nature 268, 421–422.
Strom, R.G., Malhotra, R., Ito, T., Yoshida, F., Kring, D.A., 2005. The origin of planetary impactors in the inner solar system. Science 309, 1847–1850.
Thomas, N., Barbieri, C., Keller, H.U., Lamy, P., Rickman, H., Rodrigo, R., Sierks, H., Wenzel, K.P., Cremonese, G., Jorda, L., Küppers, M., Marchi, S., Marzari, F., Massironi, M., Preusker, F., Scholten, F., Stephan, K., Barucci, M.A., Besse, S., El-Maarry, M.R., Fornasier, S., Groussin, O., Hviid, S.F., Koschny, D., Kührt, E., Martellato, E., Moissl, R., Snodgrass, C., Tubiana, C., Vincent, J.B., 2012. The geomorphology of (21) Lutetia: results from the OSIRIS imaging system onboard ESA's Rosetta spacecraft. Planet. Sp. Sci. 66, 96–124.
Thomas, N., Stelter, R., Ivanov, A., Bridges, N.T., Herkenhoff, K.E., McEwen, A.S., 2011. Spectral heterogeneity on Phobos and Deimos: HiRISE observations and comparisons to Mars Pathfinder results. Planet. Sp. Sci. 59, 1281–1292.
Thomas, P., Veverka, J., 1977. Phobos: surface density of impact craters. Icarus 30, 595–597.
Thomas, P., Veverka, J., 1980. Crater densities on the satellites of Mars. Icarus 41, 365–380.
Thomas, P.C., Robinson, M.S., 2005. Seismic resurfacing by a single impact on the asteroid 433 Eros. Nature 436, 366–369.
Vasavada, A.R., Bandfield, J.L., Greenhagen, B.T., Hayne, P.O., Siegler, M.A., Williams, J.-P., Paige, D.A., 2012. Lunar equatorial surface temperatures and regolith properties from the Diviner Lunar radiometer experiment. J. Geophys. Res.: Planets 117, E00H18.
Veverka, J., Thomas, P., Duxbury, T., 1978. The puzzling moons of Mars. Sky Telesc. 56 (1978), 186–189.
Wählisch, M., Stooke, P.J., Karachevtseva, I.P., Kirk, R., Oberst, J., Willner, K., Nadejdina, I.A., Zubarev, A.E., Konopikhin, A.A., Shingareva, K.B., 2013. Phobos and Deimos cartography. Planet. Sp. Sci..
Wählisch, M., Willner, K., Oberst, J., Matz, K.D., Scholten, F., Roatsch, T., Hoffmann, H., Semm, S., Neukum, G., 2010. A new topographic image atlas of Phobos. Earth Planet. Sci. Lett. 294, 547–553.
Werner, S.C., 2005. Major Aspects of the Chronostratigraphy and Geologic Evolutionary History of Mars (P.D. thesis), pp. 27.
Werner, S.C., Ivanov, B.A., Neukum, G., 2009. Theoretical analysis of secondary cratering on Mars and an image-based study on the Cerberus Plains. Icarus 200, 406–417.
Willner, K., Oberst, J., Hussmann, H., Giese, B., Hoffmann, H., Matz, K.D., Roatsch, T., Duxbury, T., 2010. Phobos control point network, rotation, and shape. Earth Planet. Sci. Lett. 294, 541–546.
Willner, K., Shi, X., Oberst, J., 2013. Phobos' shape and topography models. Planet. Sp. Sci..
Zahnle, K., Schenk, P., Sobieszczyk, S., Dones, L., Levison, H.F., 2001. Differential cratering of synchronously rotating satellites by ecliptic Comets. Icarus 153, 111–129.